EUROPEAN ORGANIZATION FOR NUCLEAR RESEARCH (CERN)

CERN-EP-2022-062
24 March 2022

Evidence for modification of b quark hadronization in high-multiplicity pp collisions at $\sqrt{s} = 13\,\text{TeV}$

LHCb collaboration

Abstract

The production rate of B_s^0 mesons relative to B^0 mesons is measured by the LHCb experiment in pp collisions at a center-of-mass energy $\sqrt{s} = 13\,\text{TeV}$ over the forward rapidity interval $2 < y < 4.5$ as a function of the charged particle multiplicity measured in the event. Evidence at the 3.4σ level is found for an increase of the ratio of B_s^0 to B^0 cross-sections with multiplicity at transverse momenta below 6 GeV/c, with no significant multiplicity dependence at higher transverse momentum. Comparison with data from e^+e^- collisions implies that the density of the hadronic medium may affect the production rates of B mesons. This is qualitatively consistent with the emergence of quark coalescence as an additional hadronization mechanism in high-multiplicity collisions.

Submitted to Phys. Rev. Lett.

Measurements of B mesons at colliders offer unique probes of the hadronization process by which single quarks evolve into color-neutral hadrons. In contrast to light quarks, the large mass of b quarks suppresses their production via non-perturbative processes. In addition there is no b content in the valence quark distribution of the incoming beam particles [1]. Therefore, production of $b\bar{b}$ pairs at hadron colliders is dominated by hard parton-parton interactions in the initial stages of the collisions, and is well described by perturbative QCD calculations [2–4].

The fraction of b quarks that pair with an s quark to form B_s^0 mesons, f_s, and the fraction that pair with a light d quark to form B^0 mesons, f_d, are determined through the hadronization process. One mechanism for hadronization is fragmentation, where showers of partons produced by outgoing quarks form into hadrons [5,6]. Measurements of B hadron production in e^+e^- collisions at the $\Upsilon(5S)$ [7–9] and Z^0 [10–13] resonances give consistent values for the ratio f_s/f_d, which is often interpreted as evidence for the universality of b quark fragmentation assumed by QCD factorization theorems [14]. However, measurements at the Large Hadron Collider (LHC) have shown that the ratio f_s/f_d has a dependence on the collision center-of-mass energy and the B meson transverse momentum p_{T} [15–17]. The fraction of b quarks which hadronize into baryons also varies with p_{T} [18,19]. Additionally, recent measurements have shown that charm quark hadronization differs between e^+e^- and pp collisions [20]. The reason for these variations is not immediately clear, and may be explained by hadronization mechanisms other than fragmentation [21].

An alternative hadronization process, quark coalescence, can occur when a quark produced in the collision combines with another quark to form a color singlet hadron. Models incorporating coalescence are successful at reproducing a range of measurements from fixed-target experiments and colliders [22–26]. Coalescence calculations generally require multiple quark wavefunctions to overlap in position and velocity, so the fraction of hadrons produced by this mechanism is expected to increase with the number of quarks produced in the collision. The effect is expected to be most prominent at relatively low p_{T}, which is the range where the bulk of the particles created in the collision are found. Coalescence can also lead to enhanced production of baryons at low p_{T}, and is especially important in high-energy heavy ion collisions where a large volume of deconfined quark-gluon plasma (QGP) is formed [27–29].

Recent measurements in pp collisions have shown some behaviors similar to those associated with the formation of QGP in collisions of heavy nuclei [30–32]. Among these effects is an enhanced yield of light-quark baryons and mesons with strangeness in collisions where a relatively large number of charged particles are produced [33], which was originally proposed as a QGP signature [34]. If hadronization via coalescence emerges as a mechanism for forming final state B hadrons, then the production rates of B_s^0 hadrons could increase relative to the production of B^0 hadrons as particle multiplicity increases.

This Letter describes LHCb measurements of the ratio of B_s^0 to B^0 cross sections, $\sigma_{B_s^0}/\sigma_{B^0}$, as a function of charged particle multiplicity and p_{T}. Both the B_s^0 and B^0 candidates are reconstructed through their decays to the $J/\psi\pi^+\pi^-$ final state, where the J/ψ decays into a $\mu^+\mu^-$ pair. This decay mode provides similar yields for both B_s^0 and B^0 mesons. Here multiplicity is represented by the number of charged tracks reconstructed in a silicon strip detector that surrounds the pp interaction region, the LHCb VELO detector [35,36]. These measurements use a sample of pp collisions collected at a center-of-mass energy $\sqrt{s} = 13\,\mathrm{TeV}$, corresponding to an integrated luminosity of

$5.4\ \mathrm{fb}^{-1}$.

The LHCb detector is a single-arm forward spectrometer covering the pseudorapidity range $2 < \eta < 5$, described in detail in Refs. [37, 38]. Events considered in this analysis are required to satisfy a series of triggers designed to select the decay $J/\psi \to \mu^+\mu^-$ and have one reconstructed pp interaction point (primary vertex). Each muon candidate is required to penetrate the hadron absorber layers in the LHCb muon system and have $p_{\mathrm{T}} > 500\,\mathrm{MeV}/c$. Candidate J/ψ mesons are formed from pairs of oppositely charged muon candidates that have an invariant mass near the known J/ψ mass and originate from a vertex that is displaced from the primary vertex. Charged pion candidates are identified by the response of the LHCb ring-imaging Cherenkov detectors, and are required to have total momentum $p > 3\,\mathrm{GeV}/c$ and transverse momentum $p_{\mathrm{T}} > 750\,\mathrm{MeV}/c$. Candidate $\mu^+\mu^-\pi^+\pi^-$ combinations that form a good quality common vertex are retained, and the tracks are refit with kinematic constraints that fix the $\mu^+\mu^-$ invariant mass to the known J/ψ mass, and require all four tracks to have the same origin point [39].

Simulation is required to model the effects of the detector acceptance and the selection requirements. In the simulation, pp collisions are generated using PYTHIA [40] with a specific LHCb configuration [41]. Decays of unstable particles are described by EVTGEN [42]. The interaction of the generated particles with the detector, and its response, are implemented using the GEANT4 toolkit [43] as described in Ref. [44]. The p_{T} distributions of the simulated B_s^0 and B^0 mesons, the invariant mass distributions of $\pi^+\pi^-$ pairs from their decays, and simulated event multiplicity distributions are weighted to match background-subtracted distributions that are extracted from the data using the *sPlot* method [45].

The multiplicity metrics used in this analysis are the total number of charged tracks reconstructed in the VELO detector, $\mathrm{N}_{\mathrm{tracks}}^{\mathrm{VELO}}$, and the subset of VELO tracks that point in the backward direction, away from the LHCb spectrometer, $\mathrm{N}_{\mathrm{tracks}}^{\mathrm{back}}$. The backward tracks cover a pseudorapidity interval of approximately $-3.5 < \eta < -1.5$, providing a multiplicity estimate that is measured in a different region than the signal. The VELO detector and its performance are described in detail in Refs. [35, 36]. Figure 1 shows the distributions of $\mathrm{N}_{\mathrm{tracks}}^{\mathrm{VELO}}$ and $\mathrm{N}_{\mathrm{tracks}}^{\mathrm{back}}$ for both NoBias events and B^0 signal events with one reconstructed primary vertex, which requires at least five reconstructed tracks. NoBias events are selected based on the LHC beam clock, which indicates that a bunch crossing has occurred, without any other trigger requirements. The distributions for B^0 signal events are extracted from the data, and background is removed using the *sPlot* method [45]. The results are quoted in terms of normalized multiplicity, defined as the number of tracks at the center of a given multiplicity interval divided by the mean number of tracks in NoBias events, which are $\langle \mathrm{N}_{\mathrm{tracks}}^{\mathrm{VELO}} \rangle_{\mathrm{NoBias}} = 37.7$ and $\langle \mathrm{N}_{\mathrm{tracks}}^{\mathrm{back}} \rangle_{\mathrm{NoBias}} = 11.1$, with negligibly small uncertainties. For comparison, the mean number of $\mathrm{N}_{\mathrm{tracks}}^{\mathrm{VELO}}$ and $\mathrm{N}_{\mathrm{tracks}}^{\mathrm{back}}$ are 71.1 ± 0.1 and 17.4 ± 0.3 for B^0 signal events, respectively, where the uncertainty is due to the statistical uncertainty on the track distributions. In some respects, the low- and high-multiplicity data samples approach the hadronic environments achieved in e^+e^- collisions and heavy-ion collisions, respectively.

The sample containing signal events is divided into intervals of multiplicity, and in each interval a likelihood fit is performed on the $J/\psi\pi^+\pi^-$ invariant mass spectrum to determine the ratio of B_s^0 to B^0 yields. Examples of the $J/\psi\pi^+\pi^-$ mass distribution in low- and high-multiplicity intervals are shown in Fig. 2. An increase of the B_s^0 yield relative to the B^0 yield in the high-multiplicity interval is apparent. The B_s^0 and B^0 peaks

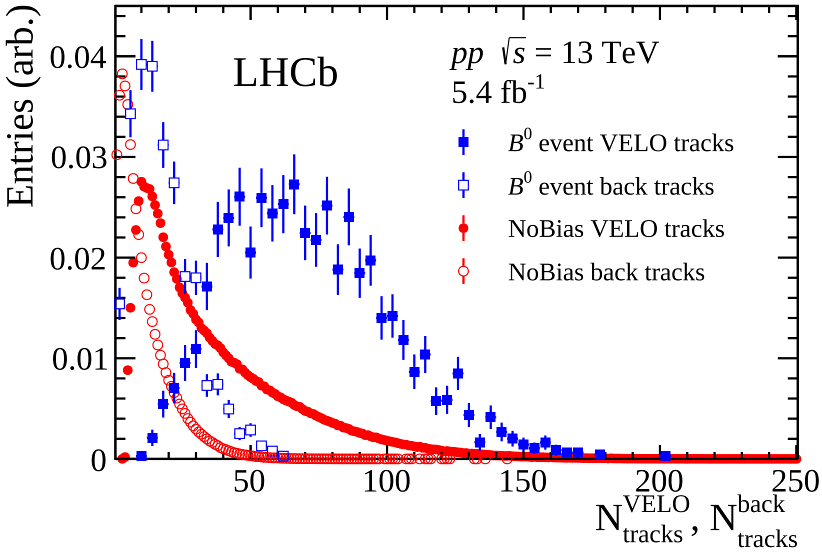

Figure 1: Distribution of the number of VELO tracks and backward tracks for NoBias events (red) and B^0 signal events (blue), each with only one primary vertex. The vertical scale is arbitrary.

are each represented in the fit by a sum of two Crystal Ball functions, which have tail parameters constrained to values determined by simulation. The background contribution is represented by an exponential function, which is found to provide a good description of the purely combinatorial $J/\psi\pi^{\pm}\pi^{\pm}$ mass spectrum with like-sign dipions. All multiplicity intervals are fit simultaneously, where the signal shapes are constrained to be the same in each interval, but their normalization and the background parameters are allowed to vary. The B_s^0 and B^0 line shapes are nearly identical, and variations of the fit functions have a negligible effect on the extracted ratio of B_s^0 to B^0 yields.

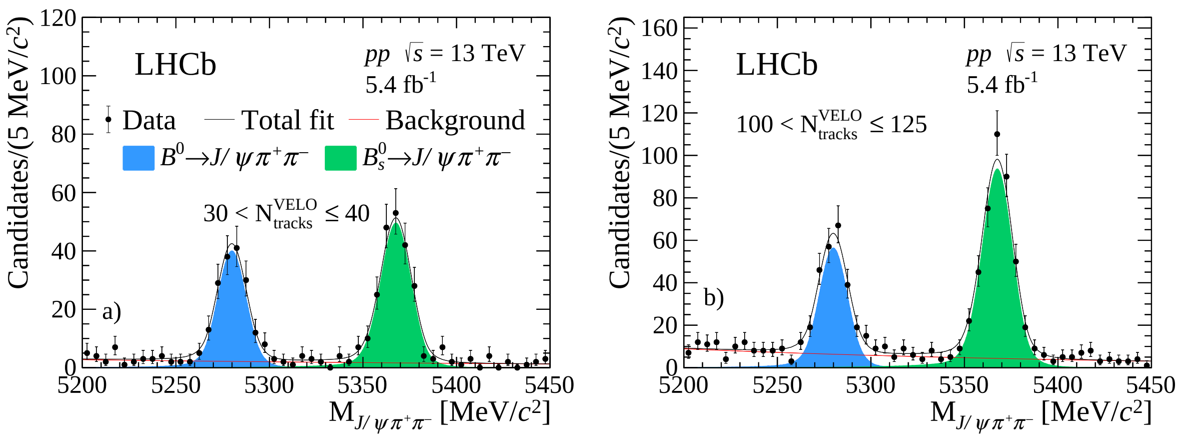

Figure 2: Measured $J/\psi\pi^+\pi^-$ invariant mass distributions and fit projections in the multiplicity ranges a) $30 < \mathrm{N}^{\mathrm{VELO}}_{\mathrm{tracks}} \leq 40$ and b) $100 < \mathrm{N}^{\mathrm{VELO}}_{\mathrm{tracks}} \leq 125$.

The ratio of cross-sections $\sigma_{B_s^0}/\sigma_{B^0}$ is found by calculating

$$\frac{\sigma_{B_s^0}}{\sigma_{B^0}} = \frac{N_{B_s^0}}{N_{B^0}} \times \frac{\mathcal{B}_{B^0}}{\mathcal{B}_{B_s^0}} \times \frac{\varepsilon_{B^0}^{\rm acc}}{\varepsilon_{B_s^0}^{\rm acc}} \times \frac{\varepsilon_{B^0}^{\rm trig}}{\varepsilon_{B_s^0}^{\rm trig}} \times \frac{\varepsilon_{B^0}^{\rm PID}}{\varepsilon_{B_s^0}^{\rm PID}} \times \frac{\varepsilon_{B^0}^{\rm reco}}{\varepsilon_{B_s^0}^{\rm reco}}, \tag{1}$$

where $N_{B_s^0}/N_{B^0}$ is the ratio of B_s^0 to B^0 signal yields returned by the fit, $\mathcal{B}_{B^0}/\mathcal{B}_{B_s^0}$ is the ratio of B^0 to B_s^0 branching fractions to $J/\psi\pi^+\pi^-$ [17,46], and $\varepsilon_{B^0}^{\rm acc}/\varepsilon_{B_s^0}^{\rm acc}$, $\varepsilon_{B^0}^{\rm trig}/\varepsilon_{B_s^0}^{\rm trig}$, $\varepsilon_{B^0}^{\rm PID}/\varepsilon_{B_s^0}^{\rm PID}$, and $\varepsilon_{B^0}^{\rm reco}/\varepsilon_{B_s^0}^{\rm reco}$ are ratios of the LHCb acceptance and the trigger, particle identification, and reconstruction efficiencies for B^0 to B_s^0 mesons, respectively. Due to the similarities of the B_s^0 and B^0 decays, many systematic uncertainties partially cancel in this ratio of cross sections. The ratio of the LHCb acceptance for the decays $\varepsilon_{B^0}^{\rm acc}/\varepsilon_{B_s^0}^{\rm acc}$ is found, using simulation, to be consistent with unity, with an uncertainty of $\sim$ 1% due to the uncertainty on the weights applied to the simulation in order to match the data. The ratio of trigger efficiencies $\varepsilon_{B^0}^{\rm trig}/\varepsilon_{B_s^0}^{\rm trig}$ is determined from data to be consistent with unity, with an uncertainty of $\sim$ 1%, using techniques described in Ref. [47], where the uncertainty comes from statistical uncertainties on the data sample. The ratio of particle identification efficiencies $\varepsilon_{B^0}^{\rm PID}/\varepsilon_{B_s^0}^{\rm PID}$ is found using calibrated samples of identified muons and pions obtained from the data, and is consistent with unity with an uncertainty of $\sim$ 1% due to the finite size of the calibration sample. The only term with a significant difference from unity is the ratio of reconstruction efficiencies, which is found to be $\varepsilon_{B^0}^{\rm reco}/\varepsilon_{B_s^0}^{\rm reco} = 0.86 \pm 0.04$ for the $p_{\rm T}$-integrated sample. This is due to the difference in the dipion mass distributions produced in the B_s^0 and B^0 decays: the B_s^0 decay is dominated by contributions from intermediate $f_0(980)$ and $f_0(1500)$ states [48], which are reconstructed with higher efficiency than the lower-mass $\rho^0(770)$ intermediate state that is significant in B^0 decays [49]. The uncertainty on this correction is due to the statistical uncertainty on the weights extracted from the data that are applied to the simulation in order to match the measured B meson $p_{\rm T}$ and dipion mass distributions.

The ratio of cross-sections for the multiplicity-integrated samples is found to be $\sigma_{B_s^0}/\sigma_{B^0} = 0.30 \pm 0.01 \pm 0.03$, where the first uncertainty is statistical and the second is systematic. This measurement agrees with previous LHCb measurements of f_s/f_d using different decay channels [17] within 1.5 standard deviations.

The multiplicity dependence of $\sigma_{B_s^0}/\sigma_{B^0}$ is shown in Fig. 3, for two different multiplicity metrics. The vertical error bars (boxes) represent point-to-point uncorrelated (fully correlated) uncertainties, while the horizontal error bars represent the bin width. Numerical values are given in the supplemental material [50]. In the left panel, the ratio shows an increasing trend with the total VELO multiplicity, where multiplicity is normalized to the mean value found in NoBias collisions. Also shown are the $\sigma_{B_s^0}/\sigma_{B^0}$ values measured in e^+e^- collisions at the $\Upsilon(5S)$ and Z^0 resonances [51], which are in good agreement with the data at low multiplicity. The right panel shows the same ratio versus the normalized $\rm N_{tracks}^{back}$. No significant dependence is observed on the multiplicity measured in the backward region. The dependence on total multiplicity, compared to the lack of dependence on multiplicity measured at backward rapidity, could indicate that the mechanism responsible for the increase in the $\sigma_{B_s^0}/\sigma_{B^0}$ ratio is related to the local particle density in a similar rapidity interval as the B mesons themselves.

The multiplicity dependence of $\sigma_{B_s^0}/\sigma_{B^0}$ is shown in three different intervals of B meson $p_{\rm T}$ in Fig. 4. Numerical values are given in the supplemental material [50]. The lowest $p_{\rm T}$ interval, $0 < p_{\rm T} < 6$ GeV/c, encompasses B mesons with $p_{\rm T}$ approximately equal to or less than their mass. In this p_{T} interval, at low multiplicity the $\sigma_{B_s^0}/\sigma_{B^0}$ ratio is consistent with values measured in e^+e^- collisions, and increases with multiplicity. The slope of a line fit to these data differs from zero by 3.4 standard deviations, thereby providing evidence for an increase of the the $\sigma_{B_s^0}/\sigma_{B^0}$ ratio. The measurements in higher p_{T} intervals, $6 < p_{\mathrm{T}} < 12$ GeV/c and $12 < p_{\mathrm{T}} < 20$ GeV/c, display no significant dependence on multiplicity and are consistent with data from e^+e^- collisions. This behavior is expected in a scenario where low-p_{T} b quarks with relatively low velocity recombine with s quarks produced in high-multiplicity collisions, while the wavefunctions of higher p_{T} b quarks have less overlap with the low-p_{T} bulk of the quarks produced in the collision. These high-p_{T} b quarks would thereby dominantly hadronize via fragmentation in vacuum, as in e^+e^- collisions, rather than via coalescence.

In summary, LHCb measurements in pp collisions at $\sqrt{s} = 13$ TeV show evidence that the production of B_s^0 mesons is enhanced relative to B^0 mesons in collisions with high charged-particle multiplicity, indicating that strangeness enhancement is present in B hadron production. In collisions with relatively low charged-particle multiplicity, and for B mesons with $p_{\mathrm{T}} > 6$ GeV/c, the rate of B_s^0 production relative to B^0 production is consistent with what is measured in e^+e^- collisions. These measurements are qualitatively consistent with expectations based on the emergence of quark coalescence as an additional hadronization mechanism, rather than fragmentation alone. These results could indicate that interactions of the b quarks with the local hadronic environment influence the hadronization process, thereby breaking factorization of b quark hadronization between e^+e^- and hadron collisions.

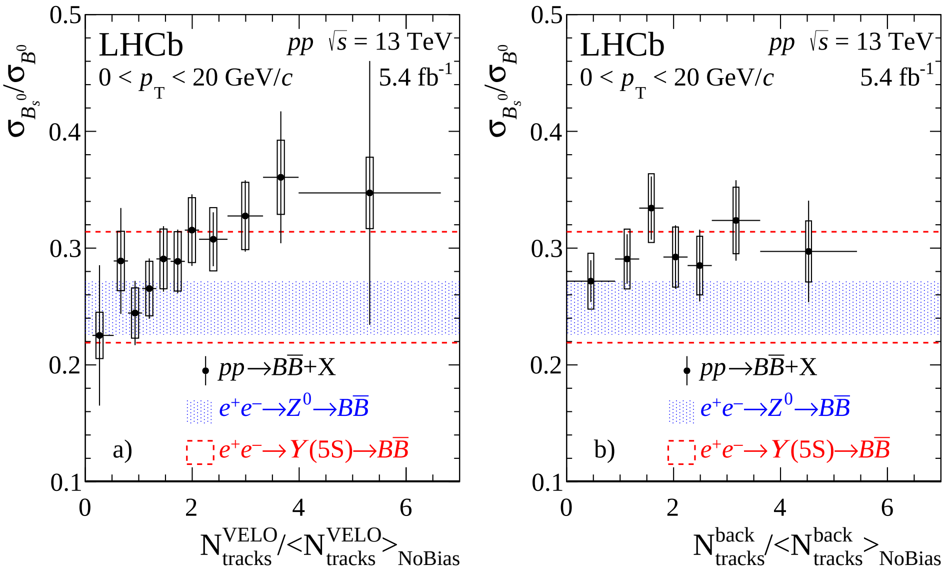

Figure 3: Ratio of cross sections $\sigma_{B_s^0}/\sigma_{B^0}$ versus the normalized multiplicity of a) all VELO tracks, and b) backward VELO tracks. The vertical error bars (boxes) represent point-to-point uncorrelated (fully correlated) uncertainties. The horizontal bands show the values measured in e^+e^- collisions.

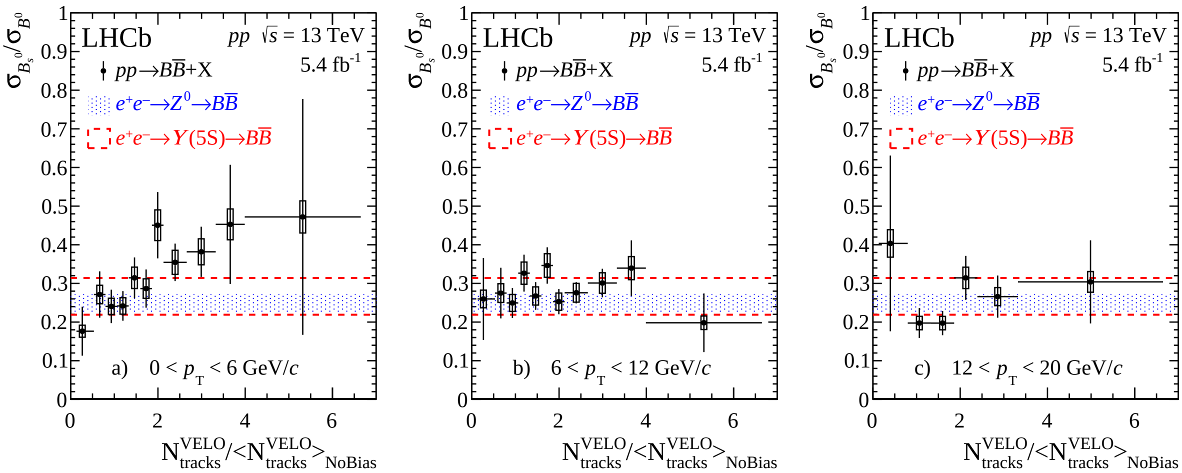

Figure 4: Ratio of cross sections $\sigma_{B_s^0}/\sigma_{B^0}$ versus normalized multiplicity in the transverse momentum ranges a) $0 < p_{\mathrm{T}} < 6$ GeV/c, b) $6 < p_{\mathrm{T}} < 12$ GeV/c, and c) $12 < p_{\mathrm{T}} < 20$ GeV/c. The vertical error bars (boxes) represent point-to-point uncorrelated (fully correlated) uncertainties. The horizontal bands show the values measured in e^+e^- collisions.

Appendix: Supplemental material

The ratio of B_s^0 to B^0 cross-sections $\sigma_{B_s^0}/\sigma_{B^0}$ versus the number of VELO tracks and number of backward VELO tracks are given in Table 1 and Table 2, respectively, for the transverse momentum range range $0 < p_{\mathrm{T}} < 20\,\mathrm{GeV}/c$. Tables 3, 4, and 5 give the ratio versus the number of VELO tracks over the transverse momentum ranges $0 < p_{\mathrm{T}} < 6\,\mathrm{GeV}/c$, $6 < p_{\mathrm{T}} < 12\,\mathrm{GeV}/c$, and $12 < p_{\mathrm{T}} < 20\,\mathrm{GeV}/c$, respectively.

Table 1: Ratio of cross-sections $\sigma_{B_s^0}/\sigma_{B^0}$ in the range $0 < p_{\mathrm{T}} < 20\,\mathrm{GeV}/c$ versus $\mathrm{N}_{\mathrm{tracks}}^{\mathrm{VELO}}$.

$\mathrm{N}_{\mathrm{tracks}}^{\mathrm{VELO}}$	$\sigma_{B_s^0}/\sigma_{B^0}$	Uncorrelated uncertainty	Correlated uncertainty
5-20	0.23	0.06	0.02
21-30	0.29	0.05	0.03
31-40	0.24	0.03	0.02
41-50	0.27	0.03	0.02
51-60	0.29	0.03	0.03
61-70	0.29	0.03	0.03
71-80	0.32	0.03	0.03
81-100	0.31	0.03	0.03
101-125	0.33	0.03	0.03
126-150	0.36	0.06	0.03
151-250	0.35	0.10	0.03

Table 2: Ratio of cross-sections $\sigma_{B_s^0}/\sigma_{B^0}$ in the range $0 < p_{\mathrm{T}} < 20\,\mathrm{GeV}/c$ versus $\mathrm{N}_{\mathrm{tracks}}^{\mathrm{back}}$.

$\mathrm{N}_{\mathrm{tracks}}^{\mathrm{back}}$	$\sigma_{B_s^0}/\sigma_{B^0}$	Uncorrelated uncertainty	Correlated uncertainty
1-10	0.27	0.02	0.02
11-15	0.29	0.02	0.03
16-20	0.33	0.03	0.03
21-25	0.29	0.03	0.03
26-30	0.29	0.03	0.03
31-40	0.32	0.03	0.03
41-60	0.30	0.04	0.03

Table 3: Ratio of cross-sections $\sigma_{B_s^0}/\sigma_{B^0}$ in the range $0 < p_{\mathrm{T}} < 6\,\mathrm{GeV}/c$ versus $\mathrm{N}_{\mathrm{tracks}}^{\mathrm{VELO}}$.

$\mathrm{N}_{\mathrm{tracks}}^{\mathrm{VELO}}$	$\sigma_{B_s^0}/\sigma_{B^0}$	Uncorrelated uncertainty	Correlated uncertainty
5-20	0.18	0.06	0.02
21-30	0.27	0.06	0.02
31-40	0.24	0.04	0.02
41-50	0.24	0.04	0.02
51-60	0.31	0.05	0.03
61-70	0.29	0.05	0.03
71-80	0.45	0.09	0.04
81-100	0.35	0.05	0.03
101-125	0.38	0.07	0.03
126-150	0.45	0.15	0.04
151-250	0.47	0.31	0.04

Table 4: Ratio of cross-sections $\sigma_{B_s^0}/\sigma_{B^0}$ in the range $6 < p_{\mathrm{T}} < 12\,\mathrm{GeV}/c$ versus $\mathrm{N}_{\mathrm{tracks}}^{\mathrm{VELO}}$.

$\mathrm{N}_{\mathrm{tracks}}^{\mathrm{VELO}}$	$\sigma_{B_s^0}/\sigma_{B^0}$	Uncorrelated uncertainty	Correlated uncertainty
5-20	0.26	0.11	0.02
21-30	0.28	0.07	0.02
31-40	0.25	0.04	0.02
41-50	0.33	0.05	0.03
51-60	0.27	0.04	0.02
61-70	0.35	0.05	0.03
71-80	0.25	0.03	0.02
81-90	0.28	0.03	0.02
101-125	0.30	0.04	0.03
126-150	0.34	0.07	0.03
151-250	0.20	0.08	0.02

Table 5: Ratio of cross-sections $\sigma_{B_s^0}/\sigma_{B^0}$ in the range $12 < p_{\mathrm{T}} < 20\,\mathrm{GeV}/c$ versus $\mathrm{N}_{\mathrm{tracks}}^{\mathrm{VELO}}$.

$\mathrm{N}_{\mathrm{tracks}}^{\mathrm{VELO}}$	$\sigma_{B_s^0}/\sigma_{B^0}$	Uncorrelated uncertainty	Correlated uncertainty
5-30	0.40	0.23	0.04
31-50	0.20	0.04	0.02
51-70	0.20	0.03	0.02
71-90	0.31	0.06	0.03
91-125	0.27	0.06	0.03
126-250	0.30	0.11	0.03

References

[1] E. Norrbin and T. Sjostrand, *Production and hadronization of heavy quarks*, Eur. Phys. J. **C17** (2000) 137, arXiv:hep-ph/0005110.

[2] LHCb collaboration, R. Aaij *et al.*, *Measurement of the b-quark production cross-section in 7 and 13 TeV pp collisions*, Phys. Rev. Lett. **118** (2017) 052002, Erratum ibid. **119** (2017) 169901, arXiv:1612.05140.

[3] LHCb collaboration, R. Aaij *et al.*, *Measurement of the $B^{\pm}$ production cross-section in pp collisions at $\sqrt{s}=7$ and 13 TeV*, JHEP **12** (2017) 026, arXiv:1710.04921.

[4] ALICE collaboration, S. Acharya *et al.*, *Measurement of beauty and charm production in pp collisions at $\sqrt{s}$ = 5.02 TeV via non-prompt and prompt D mesons*, JHEP **05** (2021) 220, arXiv:2102.13601.

[5] B. Andersson, G. Gustafson, G. Ingelman, and T. Sjostrand, *Parton fragmentation and string dynamics*, Phys. Rept. **97** (1983) 31.

[6] B. R. Webber, *A QCD model for jet fragmentation including soft gluon interference*, Nucl. Phys. **B238** (1984) 492.

[7] CLEO collaboration, M. Artuso *et al.*, *First evidence and measurement of $B_s^{(*)}\overline{B}_s^{(*)}$ production at the $\Upsilon(5S)$*, Phys. Rev. Lett. **95** (2005) 261801, arXiv:hep-ex/0508047.

[8] Belle collaboration, A. Drutskoy *et al.*, *Measurement of inclusive D_s, D^0 and J/ψ rates and determination of the $B_s^{(*)}\overline{B}_s^{(*)}$ production fraction in $b\bar{b}$ events at the $\Upsilon(5S)$ resonance*, Phys. Rev. Lett. **98** (2007) 052001, arXiv:hep-ex/0608015.

[9] CLEO collaboration, G. S. Huang *et al.*, *Measurement of $\mathcal{B}(\Upsilon(5S) \to B_s^{(*)}\overline{B}_s^{(*)})$ using ϕ mesons*, Phys. Rev. **D75** (2007) 012002, arXiv:hep-ex/0610035.

[10] OPAL collaboration, P. D. Acton *et al.*, *Evidence for the existence of the strange b flavored meson B_s^0 in Z^0 decays*, Phys. Lett. **B295** (1992) 357.

[11] ALEPH collaboration, D. Buskulic *et al.*, *Measurement of the B_s^0 lifetime and production rate with $D_s - \ell^+$ combinations in Z decays*, Phys. Lett. **B361** (1995) 221.

[12] L3 collaboration, M. Acciarri *et al.*, *Measurements of the $b\bar{b}$ production cross-section and forward backward asymmetry at center-of-mass energies above the Z pole at LEP*, Phys. Lett. **B485** (2000) 71, arXiv:hep-ex/0005023.

[13] DELPHI collaboration, J. Abdallah *et al.*, *A measurement of the branching fractions of the b quark into charged and neutral b hadrons*, Phys. Lett. **B576** (2003) 29, arXiv:hep-ex/0311005.

[14] J. C. Collins, D. E. Soper, and G. F. Sterman, *Factorization of hard processes in QCD*, Adv. Ser. Direct. High Energy Phys. **5** (1989) 1, arXiv:hep-ph/0409313.

[15] LHCb collaboration, R. Aaij *et al.*, *Measurement of the fragmentation fraction ratio f_s/f_d and its dependence on B meson kinematics*, JHEP **04** (2013) 001, arXiv:1301.5286.

[16] LHCb collaboration, R. Aaij *et al.*, *Measurement of f_s/f_u variation with proton-proton collision energy and B-meson kinematics*, Phys. Rev. Lett. **124** (2020) 122002, arXiv:1910.09934.

[17] LHCb collaboration, R. Aaij *et al.*, *Precise measurement of the f_s/f_d ratio of fragmentation fractions and of B_s^0 decay branching fractions*, Phys. Rev. **D104** (2021) 032005, arXiv:2103.06810.

[18] LHCb collaboration, R. Aaij *et al.*, *Measurement of b hadron production fractions in 7 TeV pp collisions*, Phys. Rev. **D85** (2012) 032008, arXiv:1111.2357.

[19] LHCb collaboration, R. Aaij *et al.*, *Measurement of b-hadron fractions in 13 TeV pp collisions*, Phys. Rev. **D100** (2019) 031102(R), arXiv:1902.06794.

[20] ALICE collaboration, S. Acharya *et al.*, *Charm-quark fragmentation fractions and production cross section at midrapidity in pp collisions at the LHC*, Phys. Rev. **D105** (2022) L011103, arXiv:2105.06335.

[21] A. V. Berezhnoy and A. K. Likhoded, *Relative yield of heavy hadrons as a function of the transverse momentum in LHC experiments*, Phys. Atom. Nucl. **78** (2015) 292, arXiv:1309.1979.

[22] R. Vogt and S. J. Brodsky, *QCD and intrinsic heavy quark predictions for leading charm and beauty hadroproduction*, Nucl. Phys. **B438** (1995) 261, arXiv:hep-ph/9405236.

[23] E. Braaten, Y. Jia, and T. Mehen, *The leading particle effect from heavy quark recombination*, Phys. Rev. Lett. **89** (2002) 122002, arXiv:hep-ph/0205149.

[24] R. Rapp and E. V. Shuryak, *D meson production from recombination in hadronic collisions*, Phys. Rev. **D67** (2003) 074036, arXiv:hep-ph/0301245.

[25] M. He and R. Rapp, *Hadronization and charm-hadron ratios in heavy-ion collisions*, Phys. Rev. Lett. **124** (2020) 042301, arXiv:1905.09216.

[26] V. Minissale, S. Plumari, and V. Greco, *Charm hadrons in pp collisions at LHC energy within a coalescence plus fragmentation approach*, Phys. Lett. **B821** (2021) 136622, arXiv:2012.12001.

[27] R. J. Fries, B. Muller, C. Nonaka, and S. A. Bass, *Hadronization in heavy ion collisions: recombination and fragmentation of partons*, Phys. Rev. Lett. **90** (2003) 202303, arXiv:nucl-th/0301087.

[28] V. Greco, C. M. Ko, and P. Levai, *Parton coalescence and anti-proton / pion anomaly at RHIC*, Phys. Rev. Lett. **90** (2003) 202302, arXiv:nucl-th/0301093.

[29] D. Molnar and S. A. Voloshin, *Elliptic flow at large transverse momenta from quark coalescence*, Phys. Rev. Lett. **91** (2003) 092301, arXiv:nucl-th/0302014.

[30] CMS collaboration, V. Khachatryan *et al.*, *Observation of long-range near-side angular correlations in proton-proton collisions at the LHC*, JHEP **09** (2010) 091, arXiv:1009.4122.

[31] ATLAS collaboration, G. Aad *et al.*, *Observation of long-range elliptic azimuthal anisotropies in $\sqrt{s}$ =13 and 2.76 TeV pp collisions with the ATLAS detector*, Phys. Rev. Lett. **116** (2016) 172301, arXiv:1509.04776.

[32] CMS collaboration, V. Khachatryan *et al.*, *Evidence for collectivity in pp collisions at the LHC*, Phys. Lett. **B65** (2017) 193, arXiv:1606.06198.

[33] ALICE collaboration, J. Adam *et al.*, *Enhanced production of multi-strange hadrons in high-multiplicity proton-proton collisions*, Nature Phys. **13** (2017) 535, arXiv:1606.07424.

[34] P. Koch, B. Muller, and J. Rafelski, *Strangeness in relativistic heavy ion collisions*, Phys. Rept. **142** (1986) 167.

[35] LHCb collaboration, *LHCb VELO (VErtex LOcator): Technical Design Report*, CERN-LHCC-2001-011, 2001.

[36] R. Aaij *et al.*, *Performance of the LHCb Vertex Locator*, JINST **9** (2014) P09007, arXiv:1405.7808.

[37] LHCb collaboration, A. A. Alves Jr. *et al.*, *The LHCb detector at the LHC*, JINST **3** (2008) S08005.

[38] LHCb collaboration, R. Aaij *et al.*, *LHCb detector performance*, Int. J. Mod. Phys. **A30** (2015) 1530022, arXiv:1412.6352.

[39] W. D. Hulsbergen, *Decay chain fitting with a Kalman filter*, Nucl. Instrum. Meth. **A552** (2005) 566, arXiv:physics/0503191.

[40] T. Sjöstrand, S. Mrenna, and P. Skands, *A brief introduction to PYTHIA 8.1*, Comput. Phys. Commun. **178** (2008) 852, arXiv:0710.3820; T. Sjöstrand, S. Mrenna, and P. Skands, *PYTHIA 6.4 physics and manual*, JHEP **05** (2006) 026, arXiv:hep-ph/0603175.

[41] I. Belyaev *et al.*, *Handling of the generation of primary events in Gauss, the LHCb simulation framework*, J. Phys. Conf. Ser. **331** (2011) 032047.

[42] D. J. Lange, *The EvtGen particle decay simulation package*, Nucl. Instrum. Meth. **A462** (2001) 152.

[43] Geant4 collaboration, J. Allison *et al.*, *Geant4 developments and applications*, IEEE Trans. Nucl. Sci. **53** (2006) 270; Geant4 collaboration, S. Agostinelli *et al.*, *Geant4: A simulation toolkit*, Nucl. Instrum. Meth. **A506** (2003) 250.

[44] M. Clemencic *et al.*, *The LHCb simulation application, Gauss: Design, evolution and experience*, J. Phys. Conf. Ser. **331** (2011) 032023.

[45] M. Pivk and F. R. Le Diberder, *SPlot: a statistical tool to unfold data distributions*, Nucl. Instrum. Meth. **A555** (2005) 356, arXiv:physics/0402083.

[46] Particle Data Group, P. A. Zyla *et al.*, *Review of Particle Physics*, PTEP **2020** (2020) 083C01.

[47] S. Tolk, J. Albrecht, F. Dettori, and A. Pellegrino, *Data driven trigger efficiency determination at LHCb*, LHCb-PUB-2014-039, 2014.

[48] LHCb collaboration, R. Aaij *et al.*, *Measurement of resonant and CP components in* $\overline{B}^0_s \to J/\psi\pi^+\pi^-$ *decays*, Phys. Rev. **D89** (2014) 092006, arXiv:1402.6248.

[49] LHCb collaboration, R. Aaij *et al.*, *Measurement of the resonant and CP components in* $\overline{B}^0 \to J/\psi\pi^+\pi^-$ *decays*, Phys. Rev. **D90** (2014) 012003, arXiv:1404.5673.

[50] *See Supplemental Material at [link inserted by publisher] for numerical values of cross section ratios*, .

[51] HFLAV collaboration, Y. S. Amhis *et al.*, *Averages of b-hadron, c-hadron, and* τ*-lepton properties as of 2018*, Eur. Phys. J. **C81** (2021) 226, arXiv:1909.12524.